Acta Crystallographica Section F
Structural Biology Communications
ISSN 2053-230X

High-resolution crystal structures of two crystal forms of human cyclophilin D in complex with PEG 400 molecules

Koteswara Rao Valasani,[a] Emily A. Carlson,[a] Kevin P. Battaile,[b] Andrea Bisson,[c] Chunyu Wang,[c] Scott Lovell[d] and Shirley ShiDu Yan[a]*

[a]Department of Pharmacology and Toxicology and Higuchi Bioscience Center, University of Kansas, Lawrence, KS 66047, USA, [b]IMCA-CAT, Hauptman–Woodward Medical Research Institute, 9700 South Cass Avenue, Building 435A, Argonne, IL 60439, USA, [c]Department of Biological Sciences, Center for Biotechnology and Interdisciplinary Studies, Rensselaer Polytechnic Institute, Troy, New York, USA, and [d]Protein Structure Laboratory, Del Shankel Structural Biology Center, University of Kansas, Lawrence, KS 66047, USA

Correspondence e-mail: shidu@ku.edu

Received 27 February 2014
Accepted 28 April 2014

PDB references: CypD, 4o8h; 4o8i

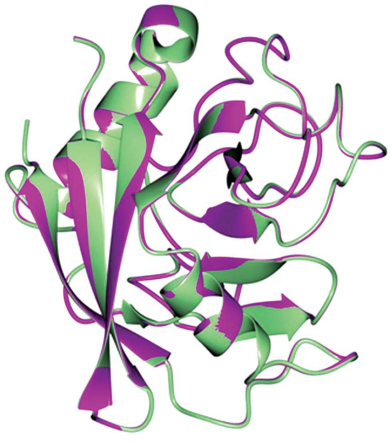

Cyclophilin D (CypD) is a key mitochondrial target for amyloid-β-induced mitochondrial and synaptic dysfunction and is considered a potential drug target for Alzheimer's disease. The high-resolution crystal structures of primitive orthorhombic (CypD-o) and primitive tetragonal (CypD-t) forms have been determined to 1.45 and 0.85 Å resolution, respectively, and are nearly identical structurally. Although an isomorphous structure of CypD-t has previously been reported, the structure reported here was determined at atomic resolution, while CypD-o represents a new crystal form for this protein. In addition, each crystal form contains a PEG 400 molecule bound to the same region along with a second PEG 400 site in CypD-t which occupies the cyclosporine A inhibitor binding site of CypD. Highly precise structural information for CypD should be extremely useful for discerning the detailed interaction of small molecules, particularly drugs and/or inhibitors, bound to CypD. The 0.85 Å resolution structure of CypD-t is the highest to date for any CypD structure.

1. Introduction

Cyclophilins are a family of proteins with peptidyl-prolyl isomerase activity, which facilitates protein folding and catalyzes the isomerization of proline residues between *cis* and *trans* isoforms (Fischer *et al.*, 1989; Galat & Metcalfe, 1995; Takahashi *et al.*, 1989; Price *et al.*, 1991; Valasani *et al.*, 2014). Proteins in the cyclophilin family are found in a variety of organisms from prokaryotes to eukaryotes (Trandinh *et al.*, 1992). In humans, 17 cyclophilin isoforms have been identified, including cyclophilin D (CypD; Davis *et al.*, 2010). In addition to the traditional peptidyl-prolyl isomerase activity, CypD is implicated in the mitochondrial permeability transition. Generally located in the mitochondrial matrix, CypD translocation to the inner mitochondrial membrane occurs upon calcium overload or oxidative stress in cells (Tanveer *et al.*, 1996; Du *et al.*, 2008, 2011). This translocation initiates the opening of the mitochondrial permeability transition pore (mPTP), classifying CypD as a modulatory component (Baines *et al.*, 2005). The mitochondrial form of CypD is encoded by the PPIF (peptidyl-prolyl isomerase F) gene, with the end product as a protein composed of 178 amino acids (Bergsma *et al.*, 1991).

The mitochondrial permeability transition is described as an increase in inner mitochondrial membrane permeability to molecules smaller than 1500 Da. This phenomenon is initiated by opening of the mPTP in cells undergoing stress, and has been linked to neuronal cell apoptosis and necrosis (Halestrap *et al.*, 2002). Opening of the mPTP leads to decreased membrane potential, disruption of calcium balance and release of apoptotic signaling molecules from the mitochondria to the cytosol to activate the apoptosis pathway. Mitochondrial swelling, outer membrane rupture and cell death *via* necrosis are common features observed following mPTP induction (Crompton, 2004; Halestrap *et al.*, 2002; Halestrap, 2005; Valasani, Chaney *et al.*, 2013; Valasani, Hu *et al.*, 2013; Valaasani *et al.*, 2014). Initially, CypD was thought to be involved in mPTP formation because of studies involving the immunosuppressive compound cyclosporine A (CsA). As CsA binds to and inhibits CypD, it desensitizes mPTP opening, resulting in reduced mitochondrial swelling, inhibition of apoptotic factor release and overall decreased

cell-death induction (Halestrap & Davidson, 1990; Takahashi *et al.*, 1989; Broekemeier *et al.*, 1989; Du *et al.*, 2008). The involvement of CypD in the mPTP was later confirmed with CypD-deficient mice as the animals were no longer susceptible to mitochondrial permeability transition induced by the addition of calcium (Schinzel *et al.*, 2005; Basso *et al.*, 2005; Du *et al.*, 2008; Du & Yan, 2010). Of all the proposed constituents of the mPTP, CypD is the only genetically confirmed component to have a significantly protective effect on calcium-induced, oxidative-stress-induced and amyloid-β (Aβ)-induced cell death (Du *et al.*, 2008, 2011, 2013; Guo *et al.*, 2013; Baines *et al.*, 2005; Nakagawa *et al.*, 2005). Several other possible candidates have been postulated, including the translocator protein (TSPO), the voltage-dependent anion channel (VDAC) and the adenine nucleotide translocase (ANT) (Zamzami *et al.*, 2005; Crompton *et al.*, 2002; Halestrap, 2006). While TSPO shows promise as a structural component (Sileikyte *et al.*, 2011), VDAC and ANT may not be essential components of the mPTP as several studies have demonstrated that cells lacking VDAC or ANT do not protect against mPTP-involved cell death (Baines *et al.*, 2007; Kokoszka *et al.*, 2004; McCommis & Baines, 2012). Although the roles of the unconfirmed constituents remain to be fully clarified in relation to the mPTP, the repositioning event of CypD has been established as a key regulator of the mPTP structural opening (Halestrap *et al.*, 1997; Connern & Halestrap, 1994; Andreeva *et al.*, 1999; Pastorino *et al.*, 1998; Crompton *et al.*, 1998; Du *et al.*, 2008; Rao *et al.*, 2013).

Recent reports suggest that a chemical alteration in the CypD configuration may fortify a cell during the event of calcium overload or oxidative stress (Baines *et al.*, 2005; Nakagawa *et al.*, 2005; Basso *et al.*, 2005). Furthermore, resistance to ischemia has been observed in both the brain (Schinzel *et al.*, 2005) and heart (Nakagawa *et al.*, 2005; Baines *et al.*, 2005) of CypD knockout mice. In addition to the role of mPTP formation in ischemia, it has been implicated in a variety of diseases, including neurodegeneration, such as Parkinson's disease (PD; Gandhi *et al.*, 2009), Huntington's disease (HD; Brustovetsky *et al.*, 2003), amyotrophic lateral sclerosis (ALS; Martin *et al.*, 2009) and Alzheimer's disease (AD; Du *et al.*, 2008). In all of these diseases many mitochondrial alterations have been discovered which aid in mPTP induction. For instance, mutations in mitochondrial DNA and proteins have been identified in PD research, alterations in striatal mitochondrial CypD levels compared with cortical mitochondria in HD pathogenesis, and changes in mitochondrial respiratory-chain enzymes and cell-death proteins have been found in ALS research. Similarly, the involvement of the mPTP is demonstrated in AD by modifications to enzymes involved in oxidative phosphorylation, oxidative stress and mitochondrial binding of Aβ. Aβ excess within neuronal mitochondria is a common feature among AD patients, and Aβ aggregation promotes events of high oxidative stress. Notably, the absence of CypD allows neuronal cell protection in an environment rich in Aβ-induced oxidative stress (Du *et al.*, 2008). Thus, lack of CypD prevents cell death, reduces impaired cognitive function (learning and memory) and diminishes synaptic dysfunction (Du *et al.*, 2011). Our published findings seem to support the concept that CypD is a key cellular target for Aβ-induced synaptic dysfunction. In the light of this, it is likely that the chemical inhibition of CypD could provide an alternative treatment for AD.

High-resolution structural information for these proteins would therefore be very useful to discern the binding mode of lead compounds, particularly in the early stages of drug discovery and development. Several crystal structures of the cyclophilin proteins, including that of CypD, have previously been determined (Mikol *et al.*, 1993, 1994*a*,*b*; Schlatter *et al.*, 2005; le Maire *et al.*, 2011; Kajitani *et al.*, 2008) but to lower resolution compared with the high-resolution structures presented here. Since higher resolution structural detail is always desirable, we have determined the crystal structures of two different forms (primitive tetragonal, CypD-t, and primitive orthorhombic, CypD-o) of CypD bound with PEG 400 to 1.45 Å resolution

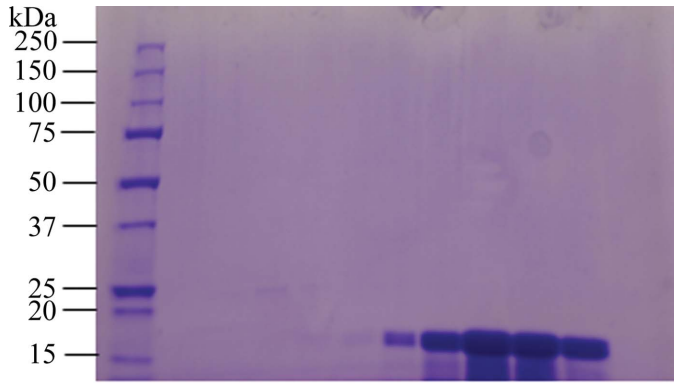

(*a*)

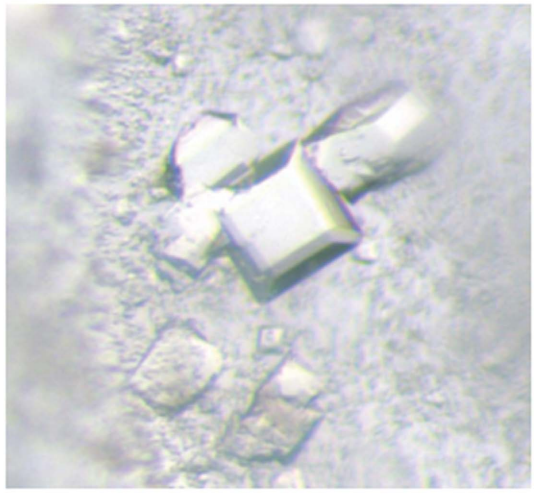

(*b*)

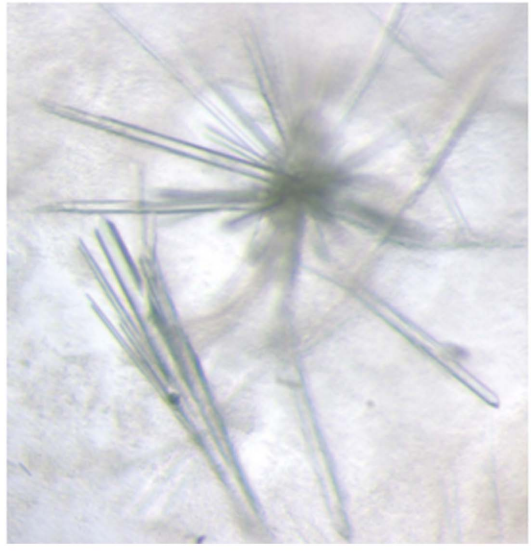

(*c*)

Figure 1
Purification and crystallization of CypD. (*a*) SDS–PAGE of purified CypD protein stained with Coomassie Brilliant Blue. Lane 1, 7.5 µg CypD protein; lane 2, 15 µg CypD protein; lane 3, 30 µg CypD protein. (*b*) CypD-t crystals obtained from ProPlex condition D1. (*c*) CypD-o cystals obtained from Wizard 3–4 condition H4.

and to the ultrahigh resolution of 0.85 Å. CypD-t is isomorphous with a previously reported structure (PDB entry 2bit, Schlatter *et al.*, 2005) in which the authors conducted an elegant series of protein mutagenesis/engineering experiments to identify a construct (K133I) that could be reproducibly crystallized as the wild-type form failed to yield crystals. However, this structure was reported to lower resolution (1.7 Å), although the sample used to determine the 2bit structure clearly diffracted to higher resolution based on the $\langle I/\sigma(I)\rangle$ in the high-resolution shell (∼10). The lower resolution reported for the structure 2bit is likely to be a consequence of hardware limitations of the in-house instrumentation used for data collection. The 0.85 Å resolution structure of CypD-t is the highest to date for any CypD structure. The second and new crystal form (CypD-o) crystallized in a primitive orthorhombic lattice and was determined to 1.45 Å resolution.

2. Materials and methods

2.1. Protein expression and purification

Escherichia coli BL21 (DE3) cells were transformed with a pET-21a-tCypD plasmid containing the truncated human peptidyl-prolyl *cis–trans*-isomerase F (CypD) with a K133I mutation to facilitate crystallization. The plasmid was a generous gift from Schlatter and coworkers (Schlatter *et al.*, 2005). Cultures were grown in Luria–Bertani (LB) medium to an A_{600} of 0.5 and were then induced with 1 m*M* isopropyl *β*-D-1-thiogalactopyranoside (IPTG). The cells were then grown overnight and harvested by centrifugation at 4000 rev min^{-1} for 30 min the following day. The cell pellet was resuspended in 50 ml 100 m*M* Tris–HCl pH 7.8, 2 m*M* EDTA, 2 m*M* DTT (per 2 l of medium) and were then lysed using sonication.

Lysates were centrifuged at 17 000 rev min^{-1} for 45 min. The soluble portion was purified on an SP-Sepharose FF column followed by anion exchange on a Q-Sepharose HP column and was then finally subjected to gel filtration on a Superdex 200 column (GE Healthcare Life Sciences). The SP column was equilibrated with 100 m*M* Tris–HCl pH 7.8, 2 m*M* EDTA, 2 m*M* DTT and the CypD protein was then eluted using an increasing gradient of 0–500 m*M* NaCl. Fractions containing the protein were collected, concentrated using ultrafiltration and then loaded onto the Q-Sepharose HP column. The Q-Sepharose HP column was equilibrated using 100 m*M* Tris–HCl pH 7.8, 2 m*M* EDTA, 2 m*M* DTT. CypD-containing fractions were collected from the flowthrough, concentrated using ultrafiltration and then applied onto a Superdex 200 column for size exclusion. The Superdex 200 column was equilibrated using 50 m*M* potassium phosphate, 100 m*M* NaCl, 2 m*M* EDTA. Peak fractions were collected and run on an SDS–PAGE gel to analyze the purity of the CypD K133I protein. The gel is shown in Fig. 1(*a*).

2.2. Crystallization and data collection

Recombinant CypD (K133I) protein was concentrated to 30 mg ml^{-1} in 50 m*M* potassium/sodium phosphate pH 7.3, 100 m*M* NaCl, 2 m*M* EDTA for crystallization. Screening was conducted in Compact Jr (Emerald Bio) sitting-drop vapor-diffusion plates at 18°C using equal volumes of protein and crystallization solutions. Tetragonal crystals (CypD-t) displaying a prismatic morphology were obtained in 1 d from condition D1 [25%(*w*/*v*) PEG 4000, 100 m*M* HEPES pH 7.5, 200 m*M* NaCl] of the ProPlex screen (Molecular Dimensions). Orthorhombic crystals (CypD-o) grew as needle clusters after 1 d from condition H4 [20%(*w*/*v*) PEG 8000, 100 m*M* Tris–HCl pH 8.5, 200 m*M* $MgCl_2$, 20%(*v*/*v*) PEG 400] of the Wizard 3–4 screen (Emerald Bio). Representative examples of these crystals are shown in Figs. 1(*b*) and 1(*c*). Single crystals of CypD-t were transferred into a fresh drop containing 75% ProPlex condition D1 and 25%(*v*/*v*) PEG 400 and cooled in liquid nitrogen prior to data collection. Crystals of CypD-o were transferred to a fresh drop of the crystallization solution (Wizard 4 condition H4), which served as the cryoprotectant for data collection. X-ray diffraction data were collected on the Advanced Photon Source IMCA-CAT beamline 17ID using a Dectris Pilatus 6M pixel-array detector. Coordinates and structure factors have been deposited in the Protein Data Bank with accession codes 4o8h (CypD-t) and 4o8i (CypD-o).

Table 1
Crystallographic data for the CypD structures.

Values in parentheses are for the highest resolution shell.

	CypD-t	CypD-o
Data collection		
Unit-cell parameters (Å)	$a = b = 57.02$, $c = 87.16$	$a = 40.56$, $b = 57.01$, $c = 57.34$
Space group	$P4_12_12$	$P2_12_12_1$
Resolution (Å)	47.72–0.85 (0.86–0.85)	40.56–1.45 (1.47–1.45)
Wavelength (Å)	1.0000	1.0000
Temperature (°C)	−173	−173
Observed reflections	1755792	155848
Unique reflections	123449	24241
$\langle I/\sigma(I)\rangle$	30.7 (1.8)	12.4 (1.8)
Completeness (%)	97.7 (60.2)	99.9 (100)
Multiplicity	14.2 (1.7)	6.4 (6.5)
R_{merge}† (%)	4.9 (34.2)	9.7 (112.0)
R_{meas}‡ (%)	5.0 (45.3)	10.6 (121.8)
$R_{p.i.m.}$‡ (%)	1.1 (29.4)	4.2 (47.1)
$CC_{1/2}$§	0.999 (0.766)	0.999 (0.715)
Refinement		
Resolution (Å)	28.51–0.85 (0.86–0.85)	33.12–1.45 (1.51–1.45)
Reflections (working/test)	117150/6189 (1964/108)	22858/1231 (2421/142)
R factor/R_{free}¶ (%)	10.7/11.9 (26.8/30.2)	16.0/19.0 (23.8/27.9)
No. of atoms		
Protein	1266	1237
PEG 400	16	10
Water	303	133
Model quality		
R.m.s. deviations		
Bond lengths (Å)	0.015	0.008
Bond angles (°)	1.482	0.909
Average B factor (Å^2)		
All atoms	8.1	19.0
Protein	5.7	17.8
PEG 400	11.1	34.6
Water	17.5	29.5
Coordinate error (maximum likelihood) (Å)	0.05	0.19
Ramachandran plot		
Most favored (%)	97.0	96.4
Additionally allowed (%)	3.0	3.6

† $R_{merge} = \sum_{hkl}\sum_i |I_i(hkl) - \langle I(hkl)\rangle|/\sum_{hkl}\sum_i I_i(hkl)$, where $I_i(hkl)$ is the intensity measured for the ith reflection and $\langle I(hkl)\rangle$ is the average intensity of all reflections with indices hkl. ‡ R_{meas} is the redundancy-independent (multiplicity-weighted) R_{merge} (Evans, 2006, 2011). $R_{p.i.m.}$ is the precision-indicating (multiplicity-weighted) R_{merge} (Diederichs & Karplus, 1997; Weiss, 2001). § $CC_{1/2}$ is the correlation coefficient of the mean intensities between two random half-sets of data (Karplus & Diederichs, 2012; Evans, 2012). ¶ R factor $= \sum_{hkl} ||F_{obs}| - |F_{calc}||/\sum_{hkl} |F_{obs}|$; R_{free} is calculated in an identical manner using 5% of randomly selected reflections that were not included in the refinement.

3. Results and discussion

3.1. Structure solution and refinement

Intensities were integrated using *XDS* (Kabsch, 2010*a*,*b*), and the Laue-class analysis and data scaling were performed with *AIMLESS* (Evans, 2011; Evans & Murshudov, 2013), which suggested that the highest probability Laue classes were 4/*mmm* (space group $P4_12_12$) for CypD-t and *mmm* (space group $P2_12_12_1$) for CypD-o. Data were truncated to a resolution where appreciable signal [$I/\sigma(I) \simeq 2.0$]

could be observed and the $CC_{1/2}$ was above 50% as indicated by the output from *AIMLESS*. The lower completeness in the outer resolution shell for CypD-t is largely a result of the instrumental setup as the high-angle diffraction was observed near the corners of the detector. Therefore, a decrease in the data completeness from 94% (0.88–0.86 Å shell) to 60% (0.86–0.85 Å shell) was observed. Structure solution for CypD-t was conducted by molecular replacement with *Phaser* (McCoy *et al.*, 2007) using a previously determined isomorphous structure of CypD (PDB entry 2bit) as the search model. All space groups with 422 point symmetry were tested and the top solution was obtained in $P4_12_12$, which was used from this point forward. For CypD-o, the same model was used for molecular-replacement searches. All space groups with 222 point symmetry were tested and the top solution was obtained in $P2_12_12_1$. Structure refinement with anisotropic atomic displacement parameters for all atoms was carried out for CypD-t with *PHENIX* (Adams *et al.*, 2010). TLS refinement (Painter & Merritt, 2006) was incorporated in the final stages of refinement with *PHENIX* for CypD-o to model anisotropic atomic displacement parameters. Manual model building was performed using *Coot* (Emsley *et al.*, 2010). Structure validation was conducted with *MolProbity* (Chen *et al.*, 2010) and figures were prepared using the *CCP4mg* package (Potterton *et al.*, 2004). Crystallographic data are provided in Table 1.

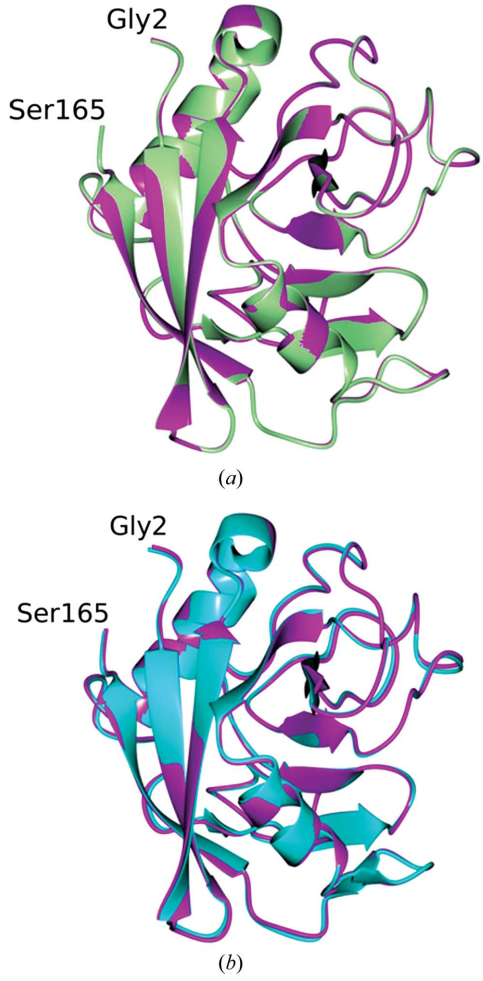

Figure 2
(*a*) Superposition of CypD-t (magenta) with 2bit (green) drawn as ribbons. The r.m.s.d. of 0.07 Å (164 residues, C^{α} atoms) indicated that the structures were basically identical. (*b*) Superposition of CypD-t (magenta) with CypD-o (cyan) drawn as ribbons.

3.2. Analysis

The unit-cell dimensions for CypD-t were nearly identical to those of the previously determined structure of CypD (PDB entry 2bit). However, given that the diffraction resolution for these crystals was the highest to date (0.85 Å) for any CypD structure, we analyzed the data/structure for any additional features. Superposition of 2bit with CypD-t using *GESAMT* (Krissinel, 2012) yielded an r.m.s.d. of 0.07 Å between C^{α} atoms (164 residues), indicating that the structures were virtually identical (Fig. 2*a*).

Examination of the electron-density maps revealed a large region of positive difference density that was ultimately assigned as a PEG 400 molecule (Fig. 3*a*) from the cryoprotectant that was bound to CypD. This PEG 400 is positioned near a hydrophobic region spanning Val93–Val97 and fits within a hydrophobic pocket on the CypD surface (Fig. 3*b*). In addition, a second PEG 400 fragment (partially disordered) was modeled as shown in Fig. 4(*a*) that forms hydrogen bonds to Arg55 and Gln63 (Fig. 4*b*), and as was observed for the ordered PEG 400 molecule, was positioned within another relatively hydrophobic cavity. Interestingly, this partially disordered PEG 400 fragment binds to the same region as was observed for CsA-bound CypD (Fig. 5) and occupies a position similar to Mva4 of the CsA inhibitor (Kajitani *et al.*, 2008). This is not too surprising given the similar hydrophobic properties of both CsA and PEG 400.

The crystal structure of CypD-o is very similar to that of CypD-t (Fig. 2*b*), with an r.m.s.d. of 0.25 Å (164 residues, C^{α} atoms) as determined by alignment with *GESAMT*. Similar to CypD-t, a large region of positive difference electron density was observed near the hydrophobic residues Val93–Val97, which was assigned as a PEG 400 molecule. However, the entire PEG molecule could not be built as a portion appeared to be disordered. Notably, the electron density

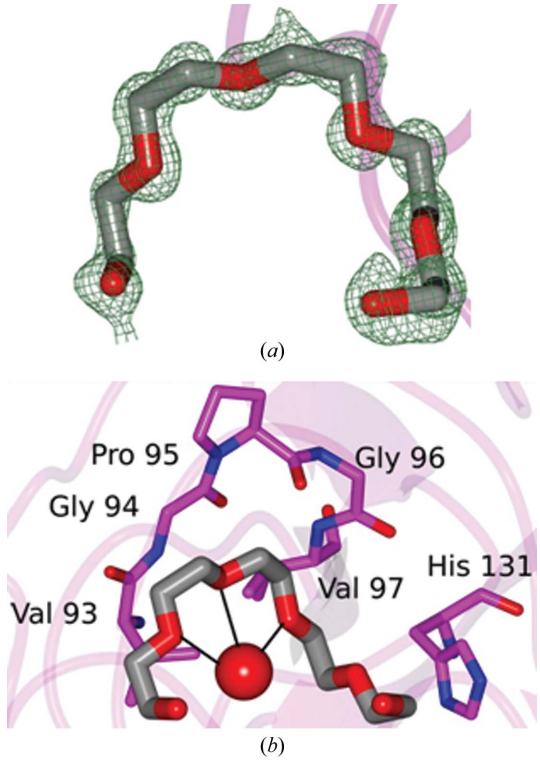

Figure 3
PEG 400 molecule bound to CypD-t. (*a*) $F_o - F_c$ electron-density map contoured at 3σ. (*b*) Hydrophobic residues that are in proximity (<4 Å) to the PEG 400 molecule. A water molecule (red sphere) is within hydrogen-bonding distance as indicated by the black lines.

present in CypD-t near Arg55 and Gln63, which was modeled as a PEG 400 fragment, was not observed in CypD-o.

Comparing the unit-cell dimensions of CypD-o (a = 40.56, b = 57.01, c = 57.34 Å; $P2_12_12_1$) with those of CypD-t (a = 57.02, b = 57.02, c = 87.16 Å; $P4_12_12$), one can see that the b and c axial lengths of the former are similar to the a and b axes of the latter. Applying the re-indexing operator ($-l$, $-k$, $-h$) to the unit cell of CypD-o would give a = 57.34, b = 57.01, c = 40.56 Å. Given that a and b axes in this transformed unit cell have a similar magnitude, one suspects that the CypD-o crystal form could be indexed in a tetragonal P lattice. If this were indeed correct, the point symmetry would be 4 with space groups $P4$, $P4_1$, $P4_2$ or $P4_3$, as the tetragonal space groups with 422 point symmetry would yield an unrealistic Matthews coefficient (V_M = 0.9 Å^3 Da^{-1}, solvent content −32.3%; Matthews, 1968). However, doubling of the c axis in the transformed unit cell would produce a lattice similar to that obtained for CypD-t, in which case space groups with 422 point symmetry could be a possibility. Analysis of the Laue symmetry using *POINTLESS* (Evans, 2006) yielded a multiplicity-weighted R factor (R_{meas}) of 22 and 28% for 4/m and 4/mmm, respectively. By contrast, the R factor for the mmm Laue class was 5% and systematic absences for 2_1 screw axes along a, b and c were present, indicating that the orthorhombic P lattice was indeed correct.

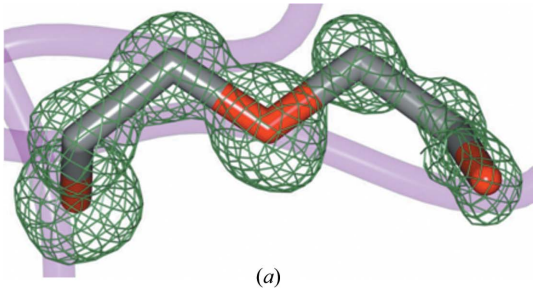

(*a*)

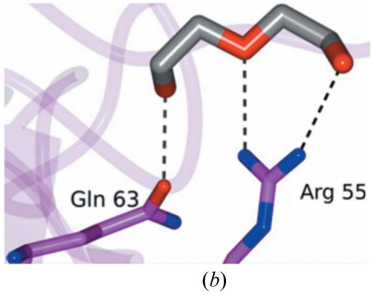

(*b*)

Figure 4
The second PEG 400 molecule fragment bound to CypD-t. (*a*) $F_o - F_c$ electron-density map contoured at 3σ. (*b*) Hydrogen bond (dashed line) between the PEG 400 fragment and CypD.

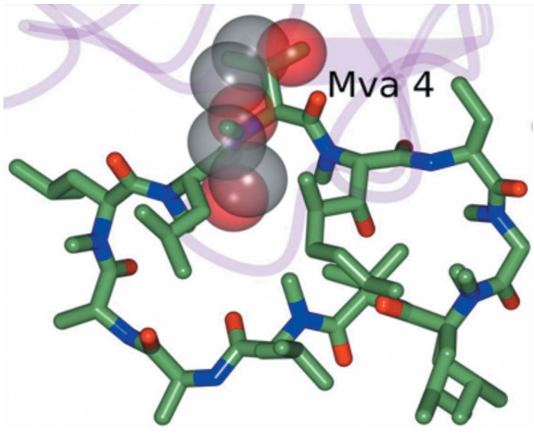

Figure 5
Superposition of the partially disordered PEG 400 molecule in CypD-t (transparent spheres) with cyclosporine A (green) bound to CypD as observed in PDB entry 2z6w (Kajitani *et al.*, 2008). The partially disordered PEG 400 molecule occupies a position similar to Mva4 of cyclosporine A as indicated. The r.m.s.d. between CypD-t and 2z6w is 0.33 Å between C$^\alpha$ atoms (164 residues).

4. Conclusions

Here, we present high-resolution crystal structures of CypD bound with PEG 400 and refined using diffraction data processed to 1.45 Å resolution and to the ultrahigh resolution of 0.85 Å. The CypD-o form crystallized in a primitive orthorhombic unit cell and represents a new crystal form of CypD. The CypD-t form, at 0.85 Å resolution, is the highest to date for any CypD structure. Our previous work has provided evidence that CypD plays a major role in Aβ-induced synaptic dysfunction in AD, making it an attractive target for drug development. Thus, the ability to acquire high-resolution structural data for various crystal forms of CypD will be useful in the initial phase of AD therapeutic development as detailed information regarding the binding mode of our lead compounds can be readily obtained.

This study was supported by grants from the National Institute of Aging (R37AG037319), the National Institute of General Medical Science (R01GM095355) and the National Institute of Neurological Disorder and Stroke (R01NS65482), and use of the University of Kansas Protein Structure Laboratory was supported by grants from the National Center for Research Resources (5P20RR017708-10) and the National Institute of General Medical Sciences (8P20GM103420-10). Use of the IMCA-CAT beamline 17-ID at the Advanced Photon Source was supported by the companies of the Industrial Macromolecular Crystallography Association through a contract with Hauptman–Woodward Medical Research Institute. Use of the Advanced Photon Source was supported by the US Department of Energy, Office of Science, Office of Basic Energy Sciences, under Contract No. DE-AC02-06CH11357. The authors have no conflict of interest to disclose.

References

Adams, P. D. *et al.* (2010). *Acta Cryst.* D**66**, 213–221.
Andreeva, L., Heads, R. & Green, C. J. (1999). *Int. J. Exp. Pathol.* **80**, 305–315.
Baines, C. P., Kaiser, R. A., Purcell, N. H., Blair, N. S., Osinska, H., Hambleton, M. A., Brunskill, E. W., Sayen, M. R., Gottlieb, R. A., Dorn, G. W., Robbins, J. & Molkentin, J. D. (2005). *Nature (London)*, **434**, 658–662.
Baines, C. P., Kaiser, R. A., Sheiko, T., Craigen, W. J. & Molkentin, J. D. (2007). *Nature Cell Biol.* **9**, 550–555.
Basso, E., Fante, L., Fowlkes, J., Petronilli, V., Forte, M. A. & Bernardi, P. (2005). *J. Biol. Chem.* **280**, 18558–18561.
Bergsma, D. J., Eder, C., Gross, M., Kersten, H., Sylvester, D., Appelbaum, E., Cusimano, D., Livi, G. P., McLaughlin, M. M. & Kasyan, K. (1991). *J. Biol. Chem.* **266**, 23204–23214.
Broekemeier, K. M., Dempsey, M. E. & Pfeiffer, D. R. (1989). *J. Biol. Chem.* **264**, 7826–7830.
Brustovetsky, N., Brustovetsky, T., Purl, K. J., Capano, M., Crompton, M. & Dubinsky, J. M. (2003). *J. Neurosci.* **23**, 4858–4867.
Chen, V. B., Arendall, W. B., Headd, J. J., Keedy, D. A., Immormino, R. M., Kapral, G. J., Murray, L. W., Richardson, J. S. & Richardson, D. C. (2010). *Acta Cryst.* D**66**, 12–21.
Connern, C. P. & Halestrap, A. P. (1994). *Biochem. J.* **302**, 321–324.
Crompton, M. (2004). *Aging Cell*, **3**, 3–6.
Crompton, M., Barksby, E., Johnson, N. & Capano, M. (2002). *Biochimie*, **84**, 143–152.
Crompton, M., Virji, S. & Ward, J. M. (1998). *Eur. J. Biochem.* **258**, 729–735.

Davis, T. L., Walker, J. R., Campagna-Slater, V., Finerty, P. J., Paramanathan, R., Bernstein, G., MacKenzie, F., Tempel, W., Ouyang, H., Lee, W. H., Eisenmesser, E. Z. & Dhe-Paganon, S. (2010). *PLoS Biol.* **8**, e1000439.
Diederichs, K. & Karplus, P. A. (1997). *Nature Struct. Biol.* **4**, 269–275.
Du, H., Guo, L., Fang, F., Chen, D., Sosunov, A. A., McKhann, G. M., Yan, Y., Wang, C., Zhang, H., Molkentin, J. D., Gunn-Moore, F. J., Vonsattel, J. P., Arancio, O., Chen, J. X. & Yan, S. D. (2008). *Nature Med.* **14**, 1097–1105.
Du, H., Guo, L., Wu, X., Sosunov, A. A., McKhann, G. M., Chen, J. X. & Yan, S. S. (2013). *Biochim Biophys Acta*, doi:10.1016/j.bbadis.2013.03.004.
Du, H., Guo, L., Zhang, W., Rydzewska, M. & Yan, S. (2011). *Neurobiol. Aging*, **32**, 398–406.
Du, H. & Yan, S. S. (2010). *Biochim. Biophys. Acta*, **1802**, 198–204.
Emsley, P., Lohkamp, B., Scott, W. G. & Cowtan, K. (2010). *Acta Cryst.* D**66**, 486–501.
Evans, P. (2006). *Acta Cryst.* D**62**, 72–82.
Evans, P. (2012). *Science*, **336**, 986–987.
Evans, P. R. (2011). *Acta Cryst.* D**67**, 282–292.
Evans, P. R. & Murshudov, G. N. (2013). *Acta Cryst.* D**69**, 1204–1214.
Fischer, G., Wittmann-Liebold, B., Lang, K., Kiefhaber, T. & Schmid, F. X. (1989). *Nature (London)*, **337**, 476–478.
Galat, A. & Metcalfe, S. M. (1995). *Prog. Biophys. Mol. Biol.* **63**, 67–118.
Gandhi, S., Wood-Kaczmar, A., Yao, Z., Plun-Favreau, H., Deas, E., Klupsch, K., Downward, J., Latchman, D. S., Tabrizi, S. J., Wood, N. W., Duchen, M. R. & Abramov, A. Y. (2009). *Mol. Cell*, **33**, 627–638.
Guo, L., Du, H., Yan, S., Wu, X., McKhann, G. M., Chen, J. X. & Yan, S. S. (2013). *PLoS One*, **8**, e54914.
Halestrap, A. (2005). *Nature (London)*, **434**, 578–579.
Halestrap, A. P. (2006). *Biochem. Soc. Trans.* **34**, 232–237.
Halestrap, A. P. & Davidson, A. M. (1990). *Biochem. J.* **268**, 153–160.
Halestrap, A. P., McStay, G. P. & Clarke, S. J. (2002). *Biochimie*, **84**, 153–166.
Halestrap, A. P., Woodfield, K. Y. & Connern, C. P. (1997). *J. Biol. Chem.* **272**, 3346–3354.
Kabsch, W. (2010*a*). *Acta Cryst.* D**66**, 125–132.
Kabsch, W. (2010*b*). *Acta Cryst.* D**66**, 133–144.
Kajitani, K., Fujihashi, M., Kobayashi, Y., Shimizu, S., Tsujimoto, Y. & Miki, K. (2008). *Proteins*, **70**, 1635–1639.
Karplus, P. A. & Diederichs, K. (2012). *Science*, **336**, 1030–1033.
Kokoszka, J. E., Waymire, K. G., Levy, S. E., Sligh, J. E., Cai, J., Jones, D. P., MacGregor, G. R. & Wallace, D. C. (2004). *Nature (London)*, **427**, 461–465.
Krissinel, E. (2012). *J. Mol. Biochem.* **1**, 76–85.
Maire, A. le, Gelin, M., Pochet, S., Hoh, F., Pirocchi, M., Guichou, J.-F., Ferrer, J.-L. & Labesse, G. (2011). *Acta Cryst.* D**67**, 747–755.
Martin, L. J., Gertz, B., Pan, Y., Price, A. C., Molkentin, J. D. & Chang, Q. (2009). *Exp. Neurol.* **218**, 333–346.
Matthews, B. W. (1968). *J. Mol. Biol.* **33**, 491–497.
McCommis, K. S. & Baines, C. P. (2012). *Biochim. Biophys. Acta*, **1818**, 1444–1450.
McCoy, A. J., Grosse-Kunstleve, R. W., Adams, P. D., Winn, M. D., Storoni, L. C. & Read, R. J. (2007). *J. Appl. Cryst.* **40**, 658–674.
Mikol, V., Kallen, J., Pflügl, G. & Walkinshaw, M. D. (1993). *J. Mol. Biol.* **234**, 1119–1130.
Mikol, V., Kallen, J. & Walkinshaw, M. D. (1994*a*). *Proc. Natl Acad. Sci. USA*, **91**, 5183–5186.
Mikol, V., Kallen, J. & Walkinshaw, M. D. (1994*b*). *Protein Eng.* **7**, 597–603.
Nakagawa, T., Shimizu, S., Watanabe, T., Yamaguchi, O., Otsu, K., Yamagata, H., Inohara, H., Kubo, T. & Tsujimoto, Y. (2005). *Nature (London)*, **434**, 652–658.
Painter, J. & Merritt, E. A. (2006). *Acta Cryst.* D**62**, 439–450.
Pastorino, J. G., Chen, S. T., Tafani, M., Snyder, J. W. & Farber, J. L. (1998). *J. Biol. Chem.* **273**, 7770–7775.
Potterton, L., McNicholas, S., Krissinel, E., Gruber, J., Cowtan, K., Emsley, P., Murshudov, G. N., Cohen, S., Perrakis, A. & Noble, M. (2004). *Acta Cryst.* D**60**, 2288–2294.
Price, E. R., Zydowsky, L. D., Jin, M. J., Baker, C. H., McKeon, F. D. & Walsh, C. T. (1991). *Proc. Natl Acad. Sci. USA*, **88**, 1903–1907.
Rao, V. K., Carlson, E. A. & Yan, S. S. (2013). *Biochim. Biophys. Acta*, doi:10.1016/j.bbadis.2013.09.003.
Schinzel, A. C., Takeuchi, O., Huang, Z., Fisher, J. K., Zhou, Z., Rubens, J., Hetz, C., Danial, N. N., Moskowitz, M. A. & Korsmeyer, S. J. (2005). *Proc. Natl Acad. Sci. USA*, **102**, 12005–12010.
Schlatter, D., Thoma, R., Küng, E., Stihle, M., Müller, F., Borroni, E., Cesura, A. & Hennig, M. (2005). *Acta Cryst.* D**61**, 513–519.
Sileikyte, J., Petronilli, V., Zulian, A., Dabbeni-Sala, F., Tognon, G., Nikolov, P., Bernardi, P. & Ricchelli, F. (2011). *J. Biol. Chem.* **286**, 1046–1053.
Takahashi, N., Hayano, T. & Suzuki, M. (1989). *Nature (London)*, **337**, 473–475.
Tanveer, A., Virji, S., Andreeva, L., Totty, N. F., Hsuan, J. J., Ward, J. M. & Crompton, M. (1996). *Eur. J. Biochem.* **238**, 166–172.
Trandinh, C. C., Pao, G. M. & Saier, M. H. Jr (1992). *FASEB J.* **6**, 3410–3420.
Valaasani, K. R., Sun, Q., Hu, G., Li, J., Du, F., Guo, Y., Carlson, E. A., Gan, X. & Yan, S. S. (2014). *Curr. Alzheimer Res.* **11**, 128–136.
Valasani, K. R., Chaney, M. O., Day, V. W. & Shidu Yan, S. (2013). *J. Chem. Inf. Model.* **53**, 2033–2046.
Valasani, K. R., Hu, G., Chaney, M. O. & Yan, S. S. (2013). *Chem. Biol. Drug Des.* **81**, 238–249.
Valasani, K. R., Vangavaragu, J. R., Day, V. W. & Yan, S. S. (2014). *J. Chem. Inf. Model.* **54**, 902–912.
Weiss, M. S. (2001). *J. Appl. Cryst.* **34**, 130–135.
Zamzami, N., Larochette, N. & Kroemer, G. (2005). *Cell Death Differ.* **12**, 1478–1480.